g Factor of the ^{99}Zr $(7/2^+)$ Isomer: Monopole Evolution in the Shape-Coexisting Region

F. Boulay,[1,2,3] G. S. Simpson,[4] Y. Ichikawa,[2] S. Kisyov,[5] D. Bucurescu,[5] A. Takamine,[2] D. S. Ahn,[2] K. Asahi,[2,6] H. Baba,[2] D. L. Balabanski,[2,7] T. Egami,[2,8] T. Fujita,[2,9] N. Fukuda,[2] C. Funayama,[2,6] T. Furukawa,[2,10] G. Georgiev,[11] A. Gladkov,[2,12] M. Hass,[13] K. Imamura,[2,14] N. Inabe,[2] Y. Ishibashi,[2,15] T. Kawaguchi,[2,8] T. Kawamura,[9] W. Kim,[12] Y. Kobayashi,[16] S. Kojima,[2,6] A. Kusoglu,[11,17] R. Lozeva,[11] S. Momiyama,[18] I. Mukul,[13] M. Niikura,[18] H. Nishibata,[2,9] T. Nishizaka,[2,8] A. Odahara,[9] Y. Ohtomo,[2,6] D. Ralet,[11] T. Sato,[2,6] Y. Shimizu,[2] T. Sumikama,[2] H. Suzuki,[2] H. Takeda,[2] L. C. Tao,[2,19] Y. Togano,[6] D. Tominaga,[2,8] H. Ueno,[2] H. Yamazaki,[2] X. F. Yang,[20] and J. M. Daugas[1,2]

[1]*CEA, DAM, DIF, 91297 Arpajon cedex, France*
[2]*RIKEN Nishina Center for Accelerator-Based Science, 2-1 Hirosawa, Wako, Saitama 351-0198, Japan*
[3]*GANIL, CEA/DSM-CNRS/IN2P3, BP55027, 14076 Caen cedex 5, France*
[4]*LPSC, CNRS/IN2P3, Université Joseph Fourier Grenoble 1, INPG, 38026 Grenoble Cedex, France*
[5]*Horia Hulubei National Institute for R&D in Physics and Nuclear Engineering (IFIN-HH), 077125 Bucharest-Măgurele, Romania*
[6]*Department of Physics, Tokyo Institute of Technology, 2-12-1 Oh-okayama, Meguro, Tokyo 152-8551, Japan*
[7]*Extreme Light Infrastructure—Nuclear Physics (ELI-NP), Horia Hulubei National Institute for R&D in Physics and Nuclear Engineering (IFIN-HH), 077125 Bucharest-Măgurele, Romania*
[8]*Department of Advanced Sciences, Hosei University, 3-7-2 Kajino-cho, Koganei, Tokyo 184-8584, Japan*
[9]*Department of Physics, Osaka University, Machikaneyama 1-1 Toyonaka, Osaka 560-0034, Japan*
[10]*Department of Physics, Tokyo Metropolitan University, 1-1 Minami-Ohsawa, Hachioji, Tokyo 192-0397, Japan*
[11]*CSNSM, Université Paris-Sud, CNRS/IN2P3, Université Paris-Saclay, 91405 Orsay Campus, France*
[12]*Department of Physics, Kyungpook National University, 80 Daehak-ro, Buk-gu, Daegu 702-701, South Korea*
[13]*Department of Particle Physics, Weizmann Institute of Science, Rehovot 76100, Israel*
[14]*Department of Physics, Meiji University, 1-1-1 Higashi-Mita, Tama, Kawasaki, Kanagawa 214-8571, Japan*
[15]*Department of Physics, University of Tsukuba, 1-1-1 Tennodai, Tsukuba, Ibaraki 305-5877, Japan*
[16]*Department of Informatics and Engineering, University of Electro-Communication, 1-5-1 Chofugaoka, Chohu, Tokyo 182-8585, Japan*
[17]*Department of Physics, Faculty of Science, Istanbul University, Vezneciler/Faith, 34134 Istanbul, Turkey*
[18]*Department of Physics, University of Tokyo, 7-3-1 Hongo, Bunkyo, Tokyo 113-0033, Japan*
[19]*State Key Laboratory of Nuclear Physics and Technology, School of Physics, Peking University, Beijing 100871, China*
[20]*Instituut voor Kern- en Stralingsfysica, K.U. Leuven, Celestijnenlaan 200D, 3001 Leuven, Belgium*

(Received 22 August 2019; revised manuscript received 28 November 2019; accepted 17 December 2019; published 16 March 2020)

The gyromagnetic factor of the low-lying $E = 251.96(9)$ keV isomeric state of the nucleus ^{99}Zr was measured using the time-dependent perturbed angular distribution technique. This level is assigned a spin and parity of $J^\pi = 7/2^+$, with a half-life of $T_{1/2} = 336(5)$ ns. The isomer was produced and spin aligned via the abrasion-fission of a ^{238}U primary beam at RIKEN RIBF. A magnetic moment $|\mu| = 2.31(14)\mu_N$ was deduced showing that this isomer is not single particle in nature. A comparison of the experimental values with interacting boson-fermion model IBFM-1 results shows that this state is strongly mixed with a main $\nu d_{5/2}$ composition. Furthermore, it was found that monopole single-particle evolution changes significantly with the appearance of collective modes, likely due to type-II shell evolution.

DOI: 10.1103/PhysRevLett.124.112501

The majority of properties of atomic nuclei evolve smoothly as a function of neutron or proton number. Therefore, one of the most surprising phenomena in the whole of the nuclear landscape is the rapid ground-state shape change between ^{98}Zr and ^{100}Zr [1]. While the former is spherical, with a low-energy structure reminiscent of a doubly magic nucleus, the latter is strongly quadrupole deformed and the first few excited states correspond to those of a deformed quantum rotor. This ground-state change has been described as a quantum phase transition (QPT) [2], where the control parameter is the valence neutron number. Although this phenomenon has been known for a long time, several open questions still exist. The sudden appearance of large ground-state deformation in ^{100}Zr implies a major rearrangement of the surface nucleons; between the two ground states, however, the exact mechanisms driving this change are yet to be elucidated. Nuclei with 59 neutrons very likely lie closest to the critical point of this QPT, and detailed studies of their structure can provide crucial experimental information about the QPT.

The gyromagnetic factor (g factor) of a state is the ratio of its magnetic moment (μ) to spin (J), $g = \mu/J$. Magnetic moments are sensitive probes of the single-particle structure of a nuclear state, providing information on valence-orbit occupancies, thus configuration mixing, and can allow confirmations of spin and parity assignments. As the magnetic moment is a property only of the wave function of the state being studied, and not of transitions between levels, its value can be a key test of nuclear model predictions.

The lowest three states of ^{99}Zr have spins $1/2^+$ (0 keV), $3/2^+$ (121.7 keV), and $7/2^+$ (252.0 keV). The $7/2^+$ state decays to the $3/2^+$ level via an isomeric $E2$ transition with a reduced transition rate of $B(E2) = 1.16(3)$ Weisskopf units (W.u.). The $3/2^+$ and $1/2^+$ states are connected by a retarded $M1$ decay with $B(M1) = 0.01$ W.u. In a shell-model picture the 252.0-keV isomeric state has a main $\nu g_{7/2}$ configuration, and the ground state $\nu s_{1/2}$ [3]. The measurements of the mean square charge radii and the nuclear moments of the ground states of the odd Zr isotopes [1] are consistent with the onset of nuclear deformation previously observed in this region. The $3/2^+$ state has a more complex configuration [4]. For the 252.0-keV state, a $g_{7/2}$ assignment is at odds with data from transfer-reaction experiments, which place this orbit at 1265 keV in ^{97}Zr [5]. The experimental identification of a low-lying $g_{7/2}$ orbit would provide experimental evidence for the spin-orbit partner (SOP) mechanism between $\pi g_{9/2}$ and $\nu g_{7/2}$ orbits, proposed to be responsible for the rapid onset of deformation here [6]. Here, occupation of the $\pi g_{9/2}$ and $\nu g_{7/2}$ SOPs leads to a large gain in correlation energy, and deformed states containing these configurations dramatically drop in energy to form the ground state of ^{100}Zr. For this reason the g factor of the $7/2^+$, 252.0-keV state has been measured, allowing detailed information to be gathered on a nucleus lying close to the critical point of the spherical-deformed QPT.

The g-factor measurement of the $7/2^+$ isomeric state of ^{99}Zr was performed at BigRIPS [7] of RIKEN RI Beam Factory (RIBF) [8]. A 345-MeV/nucleon ^{238}U beam impinged on a 100-μm-thick ^{9}Be target resulting in abrasion-fission reactions. The secondary beam was purified using both 7-mm-thick and 5-mm-thick Al wedges in the $F1$ and $F5$ dispersive planes of BigRIPS, respectively. The particle identification of the fragments was performed using an ion chamber, plastic scintillators, and the position-sensitive parallel plate avalanche counters for a combination measurement of the energy loss, time of flight, and $B\rho$ [9]. The ^{99}Zr beam with spin-aligned isomers was transported to the experimental apparatus located at the $F8$ focal plane.

The g factor of ^{99m}Zr was measured by means of a method of time-differential perturbed angular distribution (TDPAD). The spin-aligned ensemble of an isomeric state induces anisotropy in the γ-ray emission. Under an external magnetic field B_0 perpendicular to the beam axis which corresponds to the spin-orientation axis, the spin precesses the ensemble

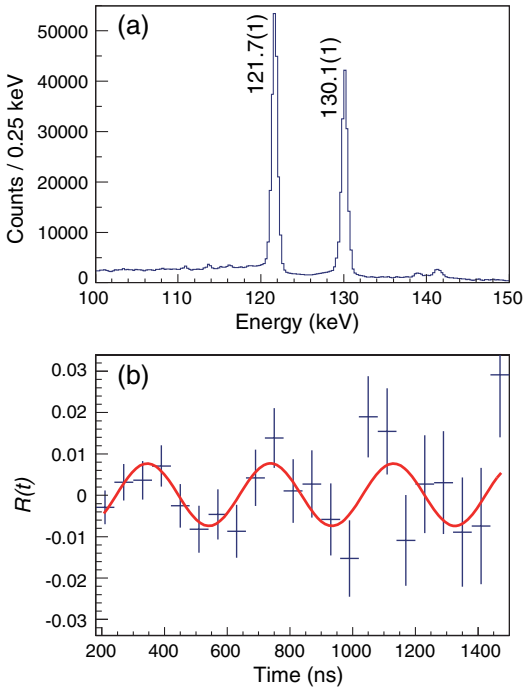

FIG. 1. (a) Energy spectrum for the two γ rays in cascade from the decay of ^{99m}Zr. (b) $R(t)$ function associated with the two γ rays.

with a Larmor frequency $\omega_L = -g\mu_N B_0/\hbar$, where g is the g factor, μ_N the nuclear magneton, and $\hbar$ the reduced Planck constant. The observation of the γ-ray anisotropy synchronized with the Larmor precession enables us to determine the g factor. The TDPAD apparatus consisted of a crystal host, a dipole electromagnet, γ-ray detectors, and a plastic scintillator. Selected fragments were implanted into an annealed Cu crystal host with a thickness of 3 mm placed between the poles of the electromagnet delivering a homogeneous magnetic field $B_0 = 250(1)$ mT. The γ rays were detected by four high-purity germanium detectors placed in a plane perpendicular to B_0 at a distance of 7.0 cm from the host and at every 90 deg. The plastic scintillator was placed in front of the implantation host and used to provide the time-zero reference. Ion-delayed γ-ray coincidences were measured on an event-by-event basis.

The γ-ray anisotropy was evaluated with an $R(t)$ function defined as

$$R(t) = \frac{I(t,\theta) - I(t,\pi/2+\theta)}{I(t,\theta) + I(t,\pi/2+\theta)}, \quad (1)$$

where $I(t,\theta)$ is the γ-ray counting rate at t time for the detector positioned at an angle θ. The $R(t)$ function corresponding to this measurement was obtained by summing for the two γ rays with energies of 121.7 and 130.1 keV in cascade below the isomeric decay, of which the measured half-life, $T_{1/2} = 336(5)$ ns, is in relatively good agreement with previous measurements [10–12].

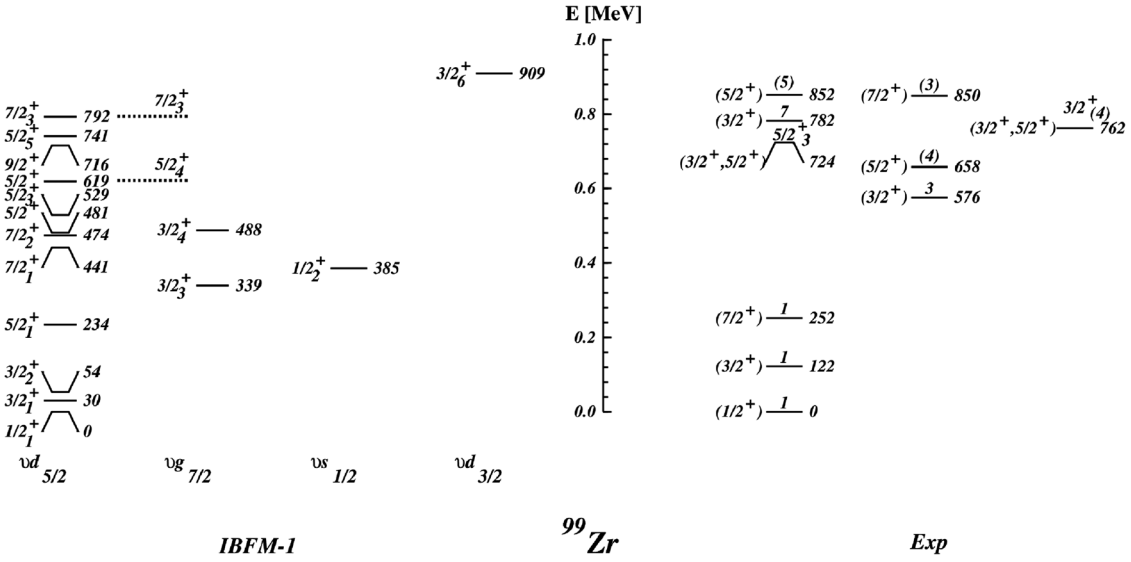

FIG. 2. A comparison between experimental low-energy level scheme of ^{99}Zr and IBFM-1 calculated states. The calculated levels are classified according to their most significant single-particle components of the wave function. Proposed correspondences between levels of the two level schemes are indicated by labeling the levels with the order number of the calculated levels of a given spin (see text for other details).

Figures 1(a) and 1(b) represent the observed γ-ray energy spectrum and the evaluated $R(t)$ function, respectively. The different multipolarities of these transitions, $M1$ and $E2$, impose a 90° phase shift in the summation. Assuming pure $M1$ and $E2$ transitions, an amount of spin alignment of 1.5(4)% is extracted. The g factor of ^{99m}Zr is determined to be $|g| = 0.66(4)$; thus, assuming a spin of $J = 7/2$, the magnetic moment of the isomeric state is $|\mu| = 2.31(14)\mu_N$. This value is far from the Schmidt value [13], $g_{\text{free}} = +0.425$, for the $\nu g_{7/2}$ orbit. In contrast, $g = +0.39(4)$ has been reported for the 1264.4-keV, $7/2_1^+$ isomer of ^{97}Zr [14]. Clearly the wave function of the $7/2^+$ isomeric state of ^{99}Zr is not a pure $(\nu g_{7/2})^1$ state.

The sensitivity of nuclear moments to the properties of the single-particle wave functions combined with the information on the collectivity of the studied state have prompted us to perform interacting boson-fermion model IBFM-1 [15,16] calculations to investigate the nuclear structure properties of the ^{99}Zr nucleus at low-excitation energies. The ODDA and PBEM programs were used [17]. The odd neutron coupled to the core was allowed to occupy the single-particle orbits $\nu d_{5/2}$, $\nu g_{7/2}$, $\nu s_{1/2}$, $\nu d_{3/2}$, and $\nu h_{11/2}$. The same parameters of the boson-fermion interaction were used in calculating both the positive- and negative-parity states. Previous IBFM calculations for ^{99}Zr [4] did not include the $\nu h_{11/2}$ orbit which is responsible for the negative-parity states, and lacked a comparison with more recent data on electromagnetic transitions and magnetic moments.

The nucleus ^{100}Zr was chosen as a core for ^{99}Zr, rather than ^{98}Zr. This is because of the significant differences between the level schemes of ^{99}Zr and the lighter odd-mass Zr isotopes. Its energy level spacings are much closer to those in the ^{100}Zr yrast band. The even-even ^{100}Zr isotope was described with the described with the interacting boson model IBM-1 [18–20] by García *et al.* in Ref. [21]. For the IBM-1 description of the ^{99}Zr core we have chosen the ^{100}Zr parameters in Ref. [21], which gives a good description of the experimental level scheme up to the 8^+ state, as well as the $E2$ transitions in the yrast band up to $J = 8$.

As quasiparticle energies and occupation probabilities in this region of rapid transitions are not known, we have adopted a set of single-particle energies (and its corresponding quasiparticle energies, calculated by BCS) which provides a good description of the properties of the lowest states ($1/2^+$, $3/2^+$, and $7/2^+$) of ^{99}Zr, that is, their known magnetic moments and electromagnetic transition probabilities, as well as a reasonably good description of the level at higher energies. In the calculations, the strength parameters used for the boson-fermion interaction (the monopole, quadrupole, and exchange terms [17]) were $A_0 = 0.08$ MeV, $\Gamma_0 = 0.3$ MeV, and $\Lambda_0 = 2.9$ MeV^2, respectively. For the electromagnetic transition operators we used equal boson and fermion effective charges of 0.159 eb for the $E2$ transitions, and for the $M1$ transitions gyromagnetic ratios of $0.4\mu_N$ and $-2.68\mu_N$ for the d boson and fermion, respectively.

Other details of these calculations are given in Ref. [22], where their results are compared to known energy levels up to higher energies (about 2 MeV) and newly determined electromagnetic transition rates. Here we emphasize the results obtained for the states at lower energies. Figure 2 shows a comparison between the IBFM-1 calculations and the experimental levels of positive parity up to about 0.8 MeV excitation energy. The IBFM-1 levels are arranged

TABLE I. Amplitudes of the components in the neutron wave functions of the first few IBFM-1 calculated positive-parity states in ^{99}Zr.

J^π	E_{expt} (keV)	E_{th} (keV)	$d_{5/2}$ (%)	$g_{7/2}$ (%)	$s_{1/2}$ (%)	$d_{3/2}$ (%)
$1/2^+$	0.0	0.0	55.7	1.0	1.5	41.8
$3/2^+$	121.7	29.9	85.2	2.1	2.2	10.6
$7/2^+$	252.0	441.9	60.6	11.1	14.9	13.4

according to the most significant single-particle components in their wave functions. The calculated positive-parity level scheme generally agrees with the experimental one, both in the predicted numbers of states of a given spin and their distribution in energy (see also Ref. [22]). The calculated level scheme is just somewhat more compressed in energy. A possible reason for this could be the choice of the core for this nucleus which is a rather difficult task for this region with significant changes between $N = 58$ and $N = 60$. For the experimental states with energy above 0.5 MeV shown in Fig. 2, the correspondence with calculated states has been made on the basis of a reasonable description of their electromagnetic decay properties, that is, branching ratios, and, when known, absolute B values [22]. The structure of the wave functions of the first few positive-parity states in ^{99}Zr is presented in Table I.

Results of the above calculations for spectroscopic quantities are compared to the experimental ones in Table II. The total experimental transition rates were obtained by correcting for unseen internal conversion contributions, calculated using the code [23]. The $B(M1; 3/2_1^+ \to 1/2_1^+)$ and $B(E2; 7/2_1^+ \to 3/2_1^+)$ reduced transition probabilities are reasonably well reproduced. Of particular interest is the good description of the magnetic moments of these states. The large magnetic moment of the $7/2^+$ isomeric state measured in the present work can be related to the contributions of the different single-particle orbits mixed in its structure. Its wave function shows (Table I) a strong admixture of the $\nu d_{5/2}$, $\nu g_{7/2}$, $\nu s_{1/2}$, and $\nu d_{3/2}$ orbits. The $1/2_1^+$ state contains large contributions from the $\nu d_{5/2}$ and $\nu d_{3/2}$ orbits, while the $3/2_1^+$ state has a relatively pure $\nu d_{5/2}$ structure. These wave function structures are also validated by the description of the transition probabilities between these levels. The calculated magnetic moments and transition probabilities of the lowest states (Table II) are rather sensitive to the values of the model parameters; therefore, the description of this experimental set of data gives some confidence in the reliability of the configurations proposed by these calculations. As the adopted J^π values of levels in ^{99}Zr [24] are given as tentative (not being based on strong arguments), we have also checked other assignments for the 252 keV state, such as the calculated $5/2_1^+$ or $5/2_2^+$ states, respectively. However, in these cases the experimental properties of this state (electromagnetic decay and magnetic moment) were not correctly described.

TABLE II. Comparison between IBFM-1 calculated and experimental transition probabilities and magnetic moments of the first three states in ^{99}Zr.

	IBFM-1	Experiment
$B(M1; 3/2_1^+ \to 1/2_1^+)$ (W.u.)	0.0109	0.0102(3)
$B(E2; 7/2_1^+ \to 3/2_1^+)$ (W.u.)	2.66	1.16(3)
μ $(1/2^+)$ (μ_N)	−1.29	−0.930(4)
μ $(3/2^+)$ (μ_N)	+0.38	+0.42(6)
μ $(7/2^+)$ (μ_N)	+2.08	±2.31(14)

The results of the IBFM-1 calculations allow insights into several interesting pieces of information regarding the structure of the low-lying states in ^{99}Zr. The origin of the delayed nature of the two transitions studied is not due to the single-particle nature of the states involved but due to their particle-hole composition. The main change between the wave functions of the $7/2^+$ and $3/2^+$ states is a 25% increase in the occupancy of the $\nu d_{5/2}$ orbit. This is supplied by roughly equal amounts of reduced population of the $\nu s_{1/2}$ and $\nu g_{7/2}$ orbits. The $\nu d_{5/2}$ and $\nu s_{1/2}$ orbits are mostly holelike in character, whereas the $\nu g_{7/2}$ orbit is particlelike. Scattering between the former and the latter is therefore strongly hindered, giving rise to the isomerism of the $7/2^+$ state. In a similar manner, increased occupation of the $\nu d_{3/2}$ orbit (particle), arising from depletion of the $\nu d_{5/2}$ (hole), retards the $M1$ transition between the first two states.

The good agreement between the calculated and experimental properties of ^{99}Zr also gives confidence in the reliability of the valence neutron single-particle energies used as input. These values can be compared to the neutron single-particle energies of the odd-A $(50 < N < 58)$ Zr isotopes experimentally determined from particle transfer reactions, which are shown in Fig. 3, plotted relative to the energy of the $\nu d_{5/2}$ orbit. In this figure one observes a steady evolution of all orbits as first the $\nu d_{5/2}$ and then the $\nu s_{1/2}$ orbits are filled. The $\nu h_{11/2}$ orbit rises in energy with increasing $\nu d_{5/2}$ occupation due to the repulsive nature of the tensor force between two $l + s$ orbits. At $N = 59$ a drastic change in the single-particle energies occurs, with the overall separation of all orbits greatly reduced. This coincides with significant occupation of the $\pi g_{9/2}$, $\nu g_{7/2}$, and $\nu h_{11/2}$ orbits, and provides evidence that monopole evolution occurs differently in collective regions.

The structure evolution of the Zr isotopes with masses around 100 was recently studied within the IBM. There are two very recent works [26,27] that use a similar approach, based on IBM calculations with configuration mixing (IBMCM). This type of calculations also correctly describes the evolution of the $A \approx 100$ even-even Zr isotopes, by a

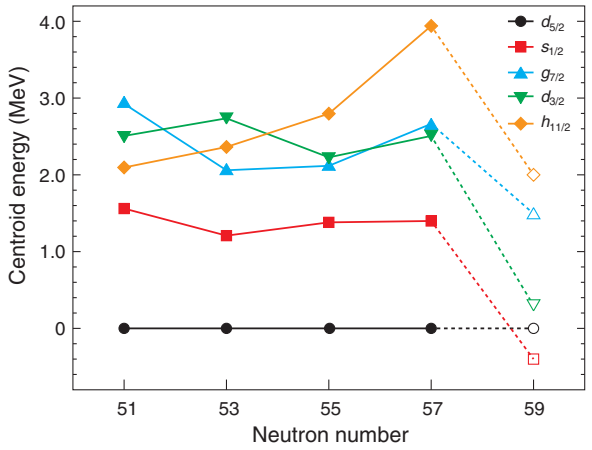

FIG. 3. Neutron single-particle energies of ^{91,93,95,97,99}Zr. For $N = 51$–57 these are experimental determinations [24,25], while for $N = 59$ the values shown are those of the present IBFM-1 calculations.

rapid lowering in energy of a deformed intruder configuration in the lighter isotopes, which becomes ground state in ^{100}Zr. The two IBMCM approaches mainly differ in the results concerning the symmetry behavior of the heavier isotopes (mass above 104), for which further experimental information is needed to disentangle the nature of their excitation. Use of an IBMCM core nucleus should lead to an improved description of ^{99}Zr by IBFM, but the lack of such a calculation code prevents this type of calculation. Instead, our present analysis allowed us to demonstrate the general behavior of the single-particle energies. It is also interesting to observe that, by adding one neutron to the spherical nucleus ^{98}Zr ^{99}Zr is driven more to the deformed side. This isotope is probably just across the critical point of the phase transition.

During the past years, many experimental studies of the even-even Zr isotopes from this mass region were made: ^{94}Zr [28], ^{96}Zr [29,30], ^{98}Zr [31,32], ^{100}Zr [33]. They documented the phenomenon of shape coexistence (the existence, at low excitation energies, of two or more structures with different quadrupole collectivities) in all these nuclei, as well as the sudden crossing in energy of two such structures between ^{98}Zr and ^{100}Zr. It has also been shown, by large-scale Monte Carlo shell-model calculations, that type-II shell evolution [34] plays a major role in the sudden onset of ground-state deformation in ^{100}Zr [35]. In type-II shell evolution, the particle-hole excitations modify the underlying shell structure, leading to a rapid onset of collective behavior.

The schematic trends of orbit evolution shown in Fig. 3 support an interpretation that at ^{99}Zr the type-II shell evolution modifies the monopole evolution of the single-particle orbits in a way different from that found in spherical regions. It also shows that mechanisms beyond just the interaction between SOPs drive the onset of collectivity.

In summary, the isomeric state of ^{99}Zr has been carefully investigated via the g-factor measurement. The reported magnetic moment $|\mu| = 2.31(14)\mu_N$ shows a value very far from the one expected for a rather pure single-particle $\nu g_{7/2}$ configuration. To shed light on the configuration of the measured isomeric state, interacting boson-fermion model IBFM-1 calculations were performed. Both g factors and $M1$ and $E2$ reduced matrix elements of the low-lying states were calculated and compared with experimental values. The $B(M1; 3/2_1^+ \rightarrow 1/2_1^+)$ and the $B(E2; 7/2_1^+ \rightarrow 3/2_1^+)$ transition probabilities are in good agreement. Moreover, the experimental g factors are also well reproduced by the IBFM-1 calculations. The wave function of the $7/2^+$ isomeric state shows a predominant $\nu d_{5/2}$ configuration. The single-particle energies adopted in our calculation can be added to the systematics of neutron single-particle energies for ^{91,93,95,97}Zr and an abrupt deviation is seen at $N = 59$. This shows that monopole evolution behaves differently in the presence of collective modes. This is likely due to the action of type-II shell evolution.

We would like to thank P. Van Isacker for fruitfull discussions. We are grateful for the technical support received from the accelerator staff of RIBF. This experiment was performed under Program No. NP1306-RIBF99 at RIBF, operated by RIKEN Nishina Center and Center for Nuclear Study, The University of Tokyo. This work was partially supported by the MEXT/JSPS KAKENHI (16K05390, 18H03692, 18H05462), and also in part by JSPS and CNRS under the Japan-France Research Cooperative Program.

[1] P. Campbell, H. L. Thayer, J. Billowes, P. Dendooven, K. T. Flanagan, D. H. Forest, J. A. R. Griffith, J. Huikari, A. Jokinen *et al.*, Phys. Rev. Lett. **89**, 082501 (2002).
[2] P. Cejnar, J. Jolie, and R. F. Casten, Rev. Mod. Phys. **82**, 2155 (2010).
[3] G. Lhersonneau, B. Pfeiffer, K.-L. Kratz, T. Enqvist, P. P. Jauho, A. Jokinen, J. Kantele, M. Leino, J. M. Parmonen, H. Penttilä, J. Äystö (the ISOLDE Collaboration), Phys. Rev. C **49**, 1379 (1994).
[4] S. Brant, V. Paar, and A. Wolf, Phys. Rev. C **58**, 1349 (1998).
[5] C. R. Bingham and G. T. Fabian, Phys. Rev. C **7**, 1509 (1973).
[6] P. Federman and S. Pittel, Phys. Lett. **69B**, 385 (1977).
[7] T. Kubo, Nucl. Instrum. Methods Phys. Res., Sect. B **204**, 97 (2003).
[8] Y. Yano, Nucl. Instrum. Methods Phys. Res., Sect. B **261**, 1009 (2007).
[9] N. Fukuda, T. Kubo, T. Ohnishi, N. Inabe, H. Takeda, D. Kameda, and H. Suzuki, Nucl. Instrum. Methods Phys. Res., Sect. B **317**, 323 (2013).

[10] H. A. Selič, G. Sadler, T. A. Khan, W.-D. Lauppe, H. Lawin, K. Sistemich, E. Monnand, J. Blachot, J. P. Bocquet, and F. Schussler, Z. Phys. A **289**, 197 (1979).
[11] J. Genevey, F. Ibrahim, J. A. Pinston, H. Faust, T. Friedrichs, M. Gross, and S. Oberstedt, Phys. Rev. C **59**, 82 (1999).
[12] J. K. Hwang, A. V. Ramayya, J. H. Hamilton, D. Fong, C. J. Beyer, P. M. Gore, E. F. Jones, Y. X. Luo, J. O. Rasmussen *et al.*, Phys. Rev. C **69**, 057301 (2004).
[13] Th. Schmidt, Z. Phys. **106**, 58 (1937).
[14] Z. Berant, R. L. Gill, M. H. Rafailovich, R. E. Chrien, J. C. Hill, F. K. Wohn, R. F. Petry, C. Chung, G. Peaslee, and M. Mohsen, Phys. Lett. **156B**, 159 (1985).
[15] F. Iachello and O. Scholten, Phys. Rev. Lett. **43**, 679 (1979).
[16] F. Iachello and P. van Isaker, *The Interacting Boson-Fermion Model* (Cambridge University Press, Cambridge, England, 1991).
[17] O. Scholten, Program package ODDA, KVI Internal Report No. 255, 1980.
[18] F. Iachello and A. Arima, Phys. Lett. **53B**, 309 (1974).
[19] A. Arima and F. Iachello, Phys. Rev. Lett. **35**, 1069 (1975).
[20] R. F. Casten and D. D. Warner, Rev. Mod. Phys. **60**, 389 (1988).
[21] J. E. García, K. Heyde, R. Fossion, V. Hellemans, and S. De Baerdemacker, Eur. Phys. J. A **26**, 221 (2005).
[22] P. Spagnoletti, G. Simpson, S. Kisyov, D. Bucurescu, J. M. Regis, N. Saed-Samii, A. Blanc, M. Jentschel, U. Köster *et al.*, Phys. Rev. C **100**, 014311 (2019).
[23] T. Kibedi, T. W. Burrows, M. B. Trzhaskovskaya, P. M. Davidson, and C. W. Nestor, Jr., Nucl. Instrum. Methods Phys. Res., Sect. A **589**, 202 (2008).
[24] Evaluated Nuclear Structure Data File (ENSDF). http://www.nndc.bnl.gov/ensdf/.
[25] E. T. Gregor, M. Scheck, R. Chapman, L. P. Gaffney, J. Keatings, K. R. Mashtakov, D. O'Donnell, J. F. Smith, P. Spagnoletti *et al.*, Eur. Phys. J. A **53**, 50 (2017).
[26] N. Gavrielov, A. Leviatan, and F. Iachello, Phys. Rev. C **99**, 064324 (2019).
[27] J. E. García-Ramos and K. Heyde, Phys. Rev. C **100**, 044315 (2019).
[28] A. Chakraborty, E. E. Peters, B. P. Crider, C. Andreoiu, P. C. Bender, D. S. Cross, G. A. Demand, A. B. Garnsworthy, P. E. Garrett *et al.*, Phys. Rev. Lett. **110**, 022504 (2013).
[29] C. Kremer, S. Aslanidou, S. Bassauer, M. Hilcker, A. Krugmann, P. von Neumann-Cosel, T. Otsuka, N. Pietralla, V. Yu. Ponomarev *et al.*, Phys. Rev. Lett. **117**, 172503 (2016).
[30] W. Witt, N. Pietralla, V. Werner, and T. Beck, Eur. Phys. J. A **55**, 79 (2019).
[31] P. Singh, W. Korten, T. W. Hagen, A. Görgen, L. Grente, M.-D. Salsac, F. Farget, E. Clément, G. de France *et al.*, Phys. Rev. Lett. **121**, 192501 (2018).
[32] W. Witt, V. Werner, N. Pietralla, M. Albers, A. D. Ayangeakaa, B. Bucher, M. P. Carpenter, D. Cline, H. M. David *et al.*, Phys. Rev. C **98**, 041302(R) (2018).
[33] W. Urban, T. Rzaca-Urban, J. Wiśniewski, I. Ahmad, A. G. Smith, and G. S. Simpson, Phys. Rev. C **99**, 064325 (2019).
[34] T. Otsuka and Y. Tsunoda, J. Phys. G **43**, 024009 (2016).
[35] T. Togashi, Y. Tsunoda, T. Otsuka, and N. Shimizu, Phys. Rev. Lett. **117**, 172502 (2016).